Hindawi
IET Signal Processing
Volume 2023, Article ID 6610762, 14 pages
https://doi.org/10.1049/2023/6610762

Research Article

Preset Conditional Generative Adversarial Network for Massive MIMO Detection

Yongzhi Yu,[1] **Shiqi Zhang**,[1] **Jiadong Shang**,[2] **and Ping Wang**[3]

[1]*Harbin Engineering University, Harbin, China*
[2]*Advanced Communication Total Technology Research Laboratory, Beijing Institute of Remote Sensing Equipment, Beijing, China*
[3]*York University, Toronto, Canada*

Correspondence should be addressed to Ping Wang; ping.wang@lassonde.yorku.ca

Received 21 June 2023; Revised 4 October 2023; Accepted 28 October 2023; Published 14 November 2023

Academic Editor: Tianyuan Liu

In recent years, extensive research has been conducted to obtain better detection performance by combining massive multiple-input multiple-output (MIMO) signal detection with deep neural network (DNN). However, spatial correlation and channel estimation errors significantly affect the performance of DNN-based detection methods. In this study, we consider applying conditional generation adversarial network (CGAN) model to massive MIMO signal detection. First, we propose a preset conditional generative adversarial network (PC-GAN). We construct the dataset with the channel state information (CSI) as a condition preset in the received signal, and train the detector without direct involvement of CSI, which effectively resists the impact of imperfect CSI on the detection performance. Then, we propose a noise removal and preset conditional generative adversarial network (NR-PC-GAN) suitable for low-signal-to-noise ratio (SNR) communication scenarios. The noise in the received signal is removed to improve the detection performance of the detector. The numerical results show that PC-GAN performs well in spatially correlated and imperfect channels. The detection performance of NR-PC-GAN is far superior to the other algorithms in low-SNR scenarios.

1. Introduction

Massive multiple-input multiple-output (MIMO) technology in wireless communications can significantly improve spectral efficiency and link reliability. Specifically, the total throughput is improved by using a large number of transmit antennas and receive antennas simultaneously for multistream communication. However, implementing massive MIMO system detection is a challenging problem [1]. Among existing detectors, maximum likelihood (ML) detection achieves the best performance, but the complexity of considering all combinations of transmission symbols during detection makes it infeasible for the practical detection. The common linear detectors based on zero-forcing (ZF) [2] and minimum mean square error (MMSE) criteria [2] require matrix inversion during detection, which becomes very complicated in massive MIMO systems with a large number of antennas. There are also suboptimal algorithms whose detection accuracy decreases significantly with the number of antennas, such as spherical decoding (SD) [3] and semidefinite relaxation (SDR) [4]. Approximate message passing (AMP) [5] and orthogonal AMP (OAMP) [6] exhibit a sharp increase in complexity in massive MIMO systems.

Deep learning (DL) has been successfully applied in areas such as computer vision, automatic speech recognition, and natural language processing [7] due to the powerful learning capability that enables it to approach the objective function step by step with nonlinear operations and neural networks. Recently, detection methods based on deep neural network (DNN) framework have also been proposed for massive MIMO detection to pursue performance enhancement [8]. DetNet with unfolding projection gradient descent method proposed in references [9, 10] achieves promising results under i.i.d. (independent and identically distributed) Rayleigh fading channel. However, due to its complexity, a longer training time is required when achieving comparable detection performance to SDR. A sparsely connected neural network (ScNet) with network simplification based on DetNet was proposed in [11], which has better detection capability than DetNet and dramatically reduces the network

complexity. However, ScNet significantly compromises detection performance in high-order scenarios, and the multisegment mapping network (MsNet) proposed in [12] uses the sigS step function to solve this problem. Both, LcgNet [13] and DL-based [14] are based on conjugate gradient descent [15] combined with DNN, and they perform similarly with large-scale antennas. Due to the algorithm model's low degree of nonlinearity, the algorithm's performance in the spatially correlated channel decreases. The OAMP-Net [16] based on the fusion of OAMP and DNN has performance advantages among existing algorithms and achieves considerable performance under both i.i.d. Rayleigh fading channel and spatially correlated channel. However, its detection process is extremely complex, making it only suitable for small systems, but not for the massive MIMO with a large number of antennas. The detection algorithm MMNet proposed in [17] is suitable for online training and has some adaptability to spatially correlated channels due to its high number of trainable variables. The authors in [18] combined deep learning and SD, proposing sparsely connected sphere decoding (SC-SD) with lower complexity. The authors in [19] proposed to combine deep reinforcement learning (DRL) with Monte Carlo tree search (MCTS) to obtain DeepMcTs detectors with better detection performance. The detection methods combining DNN framework with traditional algorithms can rely on DNN's powerful data and nonlinear expression learning ability, demonstrating superior performance over traditional algorithms. However, these algorithms are either limited by the distribution of training data or by the original algorithm model, and the detection performance decays significantly when the communication environment becomes complex; for instance increased spatial correlation, difficulty obtaining accurate channel state information (CSI), or high-noise power.

Generative adversarial network (GAN) [20] is effective in learning data distribution. Currently, GAN is widely used in computer vision, such as image restoration [21] and image super-resolution reconstruction [22]. Besides, GAN models are gradually applied in the field of communication. The authors in [23] used GAN models for modulated signal classification; the authors in [24] proposed conditional generation adversarial network- (CGAN-) based end-to-end communication for unknown channels; the authors in [25] and [26] solved the channel estimation problem with CGAN and achieved good performance gains.

Motivated by the existing work, we propose a preset conditional generative adversarial network (PC-GAN) based on CGAN for uplink massive MIMO signal detection and apply an improved U-Net [27] structure in the generator to enhance the network learning capability. In addition, to adapt the low-signal-to-noise ratio (SNR) communication scenarios, we design a noise removal and preset conditional generative adversarial network (NR-PC-GAN) detection with a denoising function. Our contributions are summarized as follows:

(1) First, we leverage the image processing method of CGAN model in the MIMO signal detection and propose a PC-GAN detection method to generate a similar probability distribution to the transmitted signal. The excellent nonlinear capability of PC-GAN enables it to release the influence of spatial correlation on the detection accuracy to a certain extent. We treat the CSI as a condition and preset it so that it is no longer directly involved in the detection process. This method can reduce the dependence of detection methods on CSI and effectively resist the impact of imperfect CSI on detection performance.

(2) The generator adopts an improved U-Net structure, which aims to improve the detection accuracy without affecting the network convergence speed, and it consists of an encoder and decoder that contain a small amount of convolution and deconvolution, respectively. Compared with the original U-Net, its computational complexity is reduced while solving the overfitting problem and improving the upper limit of detection accuracy. In addition, the improved U-Net increases the number of feature maps of the decoder, which enhances the feature reconstruction capability of the network and ensures the convergence speed of the network.

(3) An NR-PC-GAN detection method suitable for high-noise power scenarios is proposed. This detection method multiplexes the same network for noise removal and signal detection and improves detection accuracy at the expense of complexity. Simulation results show that NR-PC-GAN exhibits good noise removal capability and has superior detection performance under low-SNR conditions.

(4) The detection accuracy, complexity and robustness of the proposed PC-GAN are evaluated. The detection accuracy of PC-GAN is compared with the other detectors, and the results show that the proposed PC-GAN exhibits advantages over OAMPNet and MMNet, both in spatially correlated channels and imperfect channels. In the online training mode, the computational complexity of PC-GAN is reduced by thousands of times compared with the DNN-based detection method. In addition, PC-GAN shows good robustness when SNR and channel gain are mismatched. When the SNR conditions of training and testing are inconsistent, we call it SNR mismatch, and when the channel gain of training and testing is inconsistent, we call it channel gain mismatch.

2. Related Work

2.1. The MIMO Signal Detection Problem. In a massive MIMO system with the number of receive antennas N and the number of transmit antennas M, the received signal $\mathbf{y} \in \mathbb{C}^{N\times 1}$ is given by the following:

$$\mathbf{y} = \mathbf{H}\mathbf{x} + \mathbf{n}, \tag{1}$$

where $\mathbf{x} \in \mathbb{C}^{M\times 1}$ is the transmitted signal, $\mathbf{H} \in \mathbb{C}^{N\times M}$ denotes the channel matrix, and $\mathbf{n} \in \mathbb{C}^{N\times 1}$ is the additive Gaussian

white noise during signal transmission with zero mean and variance σ^2.

2.1.1. Linear Detection. The detection principle of the linear detection algorithm is that the final detection result is obtained by multiplying the received signal $\mathbf{y}$ by a receive filter $\mathbf{G}$. The MMSE detector can be expressed as follows:

$$\widehat{\mathbf{x}} = \mathbf{G}_{\mathrm{MMSE}}\mathbf{y} = (\mathbf{H}^{\mathbf{T}}\mathbf{H} + \sigma^2\mathbf{I})^{-1}\mathbf{H}^{\mathbf{T}}\mathbf{y}, \tag{2}$$

where $\mathbf{I}$ denotes the unit matrix of $M \times M$, $\mathbf{H}^{\mathbf{T}}$ represents the transpose of $\mathbf{H}$. It can be seen that the MMSE detection process involves matrix inversion operation. When the number of antennas in a massive MIMO system increases, the computational complexity of MMSE detection will be very high.

2.1.2. DNN-Based Detection Algorithm. Based on the projected gradient descent method, the authors in [9] used DL for MIMO detection and proposed the DetNet detection algorithm. This detection algorithm shows good performance under i.i.d. Rayleigh fading channels and achieves higher detection accuracy under low-order modulation schemes than that under high-order modulation. The DetNet detection algorithm can be described by the following equations:

$$\begin{aligned}
\mathbf{z}_k &= \rho\left(\mathbf{w}_{1k}\begin{bmatrix}\mathbf{H}^{\mathbf{T}}\mathbf{y}\\ \widehat{\mathbf{x}}_k\\ \mathbf{H}^{\mathbf{T}}\mathbf{H}\widehat{\mathbf{x}}_k\\ \mathbf{v}_k\end{bmatrix} + \mathbf{b}_{1k}\right), \\
\widehat{\mathbf{x}}_{k+1} &= \psi(\mathbf{w}_{2k}\mathbf{z}_k + \mathbf{b}_{2k}) \\
\widehat{\mathbf{v}}_{k+1} &= \mathbf{w}_{3k}\mathbf{z}_k + \mathbf{b}_{3k} \\
\widehat{\mathbf{x}}_1 &= 0
\end{aligned} \tag{3}$$

where $k = 1, \ldots, L$, L is the number of layers of the network, $\psi(\cdot)$ is a segmented symbolic mapping function similar to the hyperbolic tangent, and $[\mathbf{w}_{1k}, \mathbf{b}_{1k}, \mathbf{w}_{2k}, \mathbf{b}_{2k}, \mathbf{w}_{3k}, \mathbf{b}_{3k}]$ are trainable variables.

2.2. CGAN Model. GAN was proposed as a machine learning method in [20], which consists of two networks, the generator and the discriminator. The generator attempts to fool the discriminator by generating data similar to the real sample distribution, and the discriminator tries to distinguish the sample sources correctly. During the training process, the generator and the discriminator compete with each other, and their generation and discrimination abilities are gradually improved to Nash [28] equilibrium. The basic GAN generator synthesizes real samples from random noise; this unsupervised training process is not accessible, and the properties of the generated samples cannot be controlled. To solve this problem, an improved CGAN was proposed in [29], adding additional conditional information to the basic GAN to generate samples with specific attributes. The structure of CGAN network is shown in Figure 1, where z denotes the input noise, x is the generation target, and $\widehat{\mathbf{x}}$ is the output of the generator. The discriminator x and $\widehat{\mathbf{x}}$ judges to be real and to be fake. Condition c can be a category label or other type of data that controls sample attribute generation. The condition c is input as an independent item to the generator and discriminator.

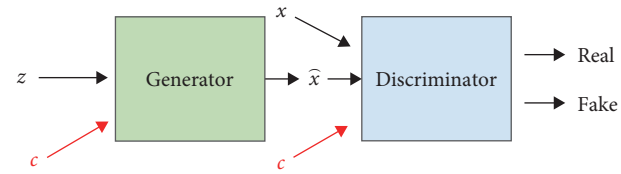

FIGURE 1: CGAN network structure.

3. Proposed PC-GAN

This section proposes a PC-GAN detection method for massive MIMO detection based on CGAN. Unlike CGAN, we preset the condition before entering it into the network for PC-GAN. We preprocess the transmitted signal, transform the transmitted signal matrix $\mathbf{X}$ and received signal matrix $\mathbf{Y}_{\mathbf{H}}$ into images, and then perform MIMO signal detection with an image-to-image conversion. In this section, we first introduce the system model, the signal image processing and the precondition construction process. Then, we detail the detection working process of PC-GAN and its structure.

3.1. System Model. As shown in Figure 2, we image the signal and solve the signal detection problem based on CGAN. We consider an uplink massive MIMO system with N antennas at the base station (BS) and M single-antenna users at the transmitter. We consider preprocessing the transmitted signal $\mathbf{x}_t$ before it passes through the channel, constructing the transmitted signal matrix $\mathbf{X} \in \mathbb{C}^{M\times P}$ (P is the number of upsampling points), and transmitting the signal through the channel to the BS to obtain the received signal matrix $\mathbf{Y}_{\mathbf{H}} \in \mathbb{C}^{N\times P}$. Thus, Equation (1) can be written as follows:

$$\mathbf{Y}_{\mathbf{H}} = \mathbf{H}\mathbf{X} + \mathbf{n}_1, \tag{4}$$

where $\mathbf{H}$ is the channel matrix, and $\mathbf{n}_1 \in \mathbb{C}^{N\times P}$ represents the additive Gaussian white noise. Then, we use the CGAN-based detection network to obtain the transmitted signal $\mathbf{X}$ from the received signal $\mathbf{Y}_{\mathbf{H}}$ to complete the signal detection.

3.2. Image Processing and Condition Presetting. In the massive MIMO detection problem, the original transmitted signal $\mathbf{x}_t$ is usually considered as a modulated signal of dimension $M \times 1$. The principle of PC-GAN for MIMO signal detection is image feature extraction and reconstruction. The essence of an image is a matrix, and the characteristics of the image are closely related to the relationship between the elements in the matrix. However, the transmitted signals are M mutually independent symbols, and to establish the connection between the transmitted signals, we consider the preprocessing of $\mathbf{x}_t$. First, we upsample $\mathbf{x}_t$ to get the sampled signal matrix $\mathbf{x}_{\mathrm{up}} \in \mathbb{C}^{M\times P}$. Then, with the help of a high-

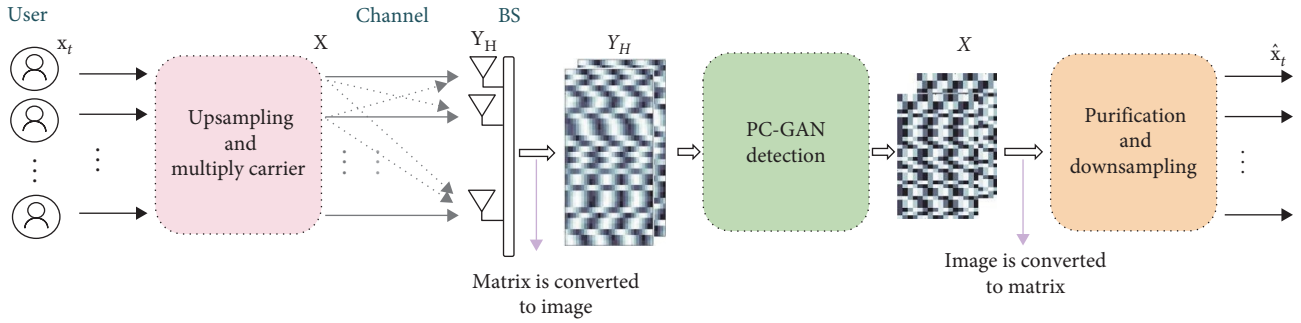

FIGURE 2: Signal detection framework for massive MIMO systems.

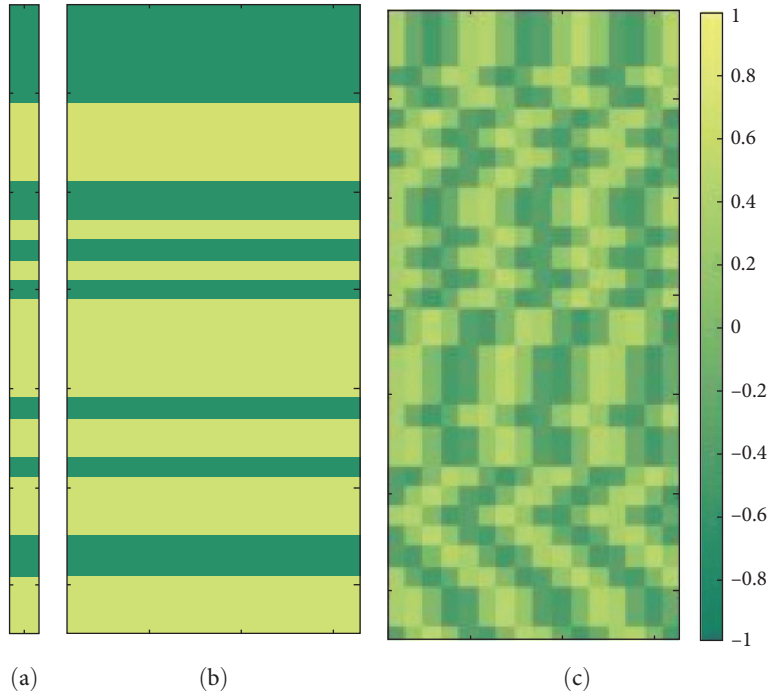

FIGURE 3: The real part image of (a) original transmit signal $\mathbf{x}_t$, (b) upsampling signal $\mathbf{x}_{\text{up}}$, and (c) transmit signal matrix $\mathbf{X}$.

frequency sinusoidal carrier, we can get the transmitted signal matrix $\mathbf{X} \in \mathbb{C}^{M \times P}$ with a close correlation between the elements. The correlation between the elements of the signal matrix can be intuitively determined from the real part image of the signal matrix in Figure 3. It can be seen that the image of the transmitted signal matrix $\mathbf{X}$ after preprocessing has certain texture characteristics, and we can complete the signal detection work based on the texture characteristics of the image.

The channel matrix in MIMO communication is the bridge between the received signal and the transmitted signal. In the PC-GAN detection method, we consider the channel matrix as conditional information to control the process of obtaining the transmitted signal from the received signal. The intuition behind this is that the conditional input term in CGAN can control the network to generate samples with the specific properties. The principle of existing MIMO detection methods, both traditional and DNN-based methods, is to calculate the transmitted signal based on the received signal and the channel matrix. In MIMO communication, the signal received by the BS is obtained by transmitting the transmitted signal through the channel, which means that the received signal is related to the channel matrix. Based on this theory, we propose a detection network that only needs to provide received signal. In order to train a detection network that no longer needs to provide channel matrix separately, we perform conditional presetting when constructing the training set. First, we simulate the transmitted signal matrix $\mathbf{X} \in \mathbb{C}^{M \times P}$, collect the conditional information channel matrix $\mathbf{H}$, and then preset the condition $\mathbf{H}$ in the received signal $\mathbf{Y_H} \in \mathbb{C}^{N \times P}$ using Equation (4). We transform $\mathbf{X}$ and $\mathbf{Y_H}$ into image tensor X and Y_H with dual channel of real and imaginary parts and construct training sets with X and Y_H. The dimensions of X and Y_H are $M \times P \times 2$ and $N \times P \times 2$, respectively. During network training, the CGAN in Figure 1 needs to input additional conditions into the generator and discriminator. The input Y_H of

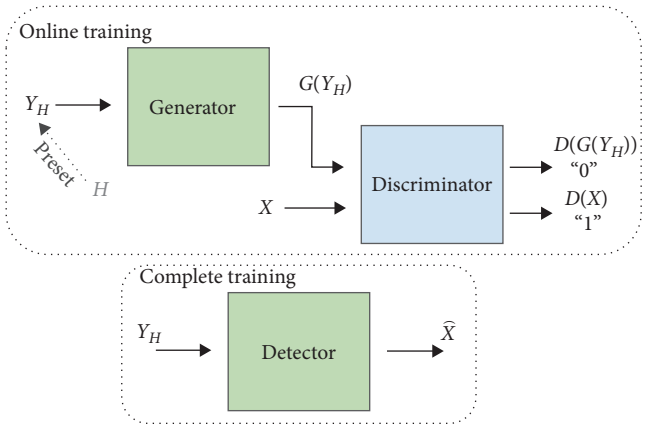

FIGURE 4: Description of the PC-GAN detection method.

the PC-GAN generator is already preset with condition **H**, so the generator does not need additional conditional input. In addition, when constructing the dataset, we ensure that X and Y_H correspond strictly so that the discriminator does not require additional conditional input. The purpose of conditional presetting is to reduce the dependence on the channel matrix **H** in the detection process, so that the detection method can be adapted to imperfect CSI and, at the same time, simplify the network input.

3.3. The Working Process of PC-GAN Detection. In our work, we use PC-GAN to build the mapping relationship from the received signal image Y_H to the transmitted signal image X. As shown in Figure 4, we input Y_H into the generator and X into the discriminator for PC-GAN training. We use the generator that has completed the training as the PC-GAN detector, which can convert the received signal image Y_H to the transmitted signal image X.

During the training period, the generator performs feature extraction and feature reconstruction on the received signal image Y_H, and then generates the signal image $G(Y_H)$. We collect $G(Y_H)$ and X to train the discriminator's ability to distinguish the real samples from the generated samples. If the discriminator can successfully distinguish $G(Y_H)$ and X, the result is fed back to the generator to obtain the gradients of the two networks. The generator and discriminator continuously perform max–min games, and the signal image $G(Y_H)$ generated by the generator gradually approaches the real transmitted signal image X, until the discriminator is unable to distinguish the generated samples from the real samples, and then the training ends. We apply the following loss function to achieve the optimization of the PC-GAN detection method:

$$\max_D \min_G L(D,G) = E[\log D(X)] + E[\log(1 - D(G(Y_H)))], \tag{5}$$

where $D(X)$ and $D(G(Y_H))$ are the outputs of the discriminator. In the training process, we record $D(X)$ as label "1" and $D(G(Y_H))$ as label "0". When the discriminator can not distinguish the generated samples from the real samples, the network training can be completed. We can use the trained generator to perform MIMO detection, in the case of inputting a new received signal image Y_H.

3.4. Generator and Discriminator Structure. The core idea of our work is to transform the received signal image Y_H into the transmitted signal image X. This process requires feature extraction and feature reconstruction for Y_H. We use an improved U-Net in the generator. U-Net is a variant of FCN [30], which can be trained completely with fewer samples. Unlike only one deconvolution of the encoder in FCN, the encoder on the left of U-Net is strictly opposite to the encoder on the right, which enhances the U-Net's ability for the feature recovery.

We made some adjustments to the U-Net, and the improved structure of U-Net is shown in Figure 5(a). We consider a 3-layer U-shaped structure. The improved U-Net simplifies the convolution operation to reduce the computational complexity while avoiding model overfitting. A size adjuster containing convolution and deconvolution layers is designed to shape the input Y_H to the same size as X, so that the detection system can be applied to a multi-antenna system. The encoder consists of batch normalization, convolution, and ReLU activation functions, and the decoder consists of batch normalization, deconvolution, and ReLU activation functions. The convolution operation is used for the feature extraction, and the deconvolution operation is used for the feature reconstruction. The batch normalization is used to continuously adjust the intermediate output of the neural network to make the neural network more stable. Setting the ReLU activation function both avoids gradient vanishing and enhances the nonlinear capability of the network. In addition, we set buffer blocks to avoid convergence difficulties caused by too-deep feature extraction.

Our detection work essentially establishes the mapping function from Y_H to X. The mapping relation from Y_H to X is more complicated than the mapping relation from noisy image to noiseless image. So, if the role of the decoder in the image denoising process is considered as feature recovery, then it is regarded as feature reconstruction in the process of MIMO detection. We consider increasing the number of feature maps in the decoder to enhance the feature reconstruction capability of the network. As shown in Figure 5(a), the convolution step in the first layer of the encoder is 2×2 and the number of feature maps is 64, whereas the deconvolution step in the first layer of the decoder is 2×2 and the number of feature maps is 128. It shows that the number of encoder and decoder feature maps of the improved U-Net is no longer completely symmetrical. In addition, the size of the convolution and deconvolution kernels used is 3×3, and the small convolution kernels can enhance the nonlinear capability of the network. Further, the improved U-Net retains the skipping connection to fuze the multiscale features and accelerates the convergence speed.

The discriminator structure is shown in Figure 5(b). We use the patch architecture [31] with three convolution layers and one fully connected layer. The output of the regular discriminator is a single evaluation value, but the patch architecture maps the input to a receptive field, which is averaged

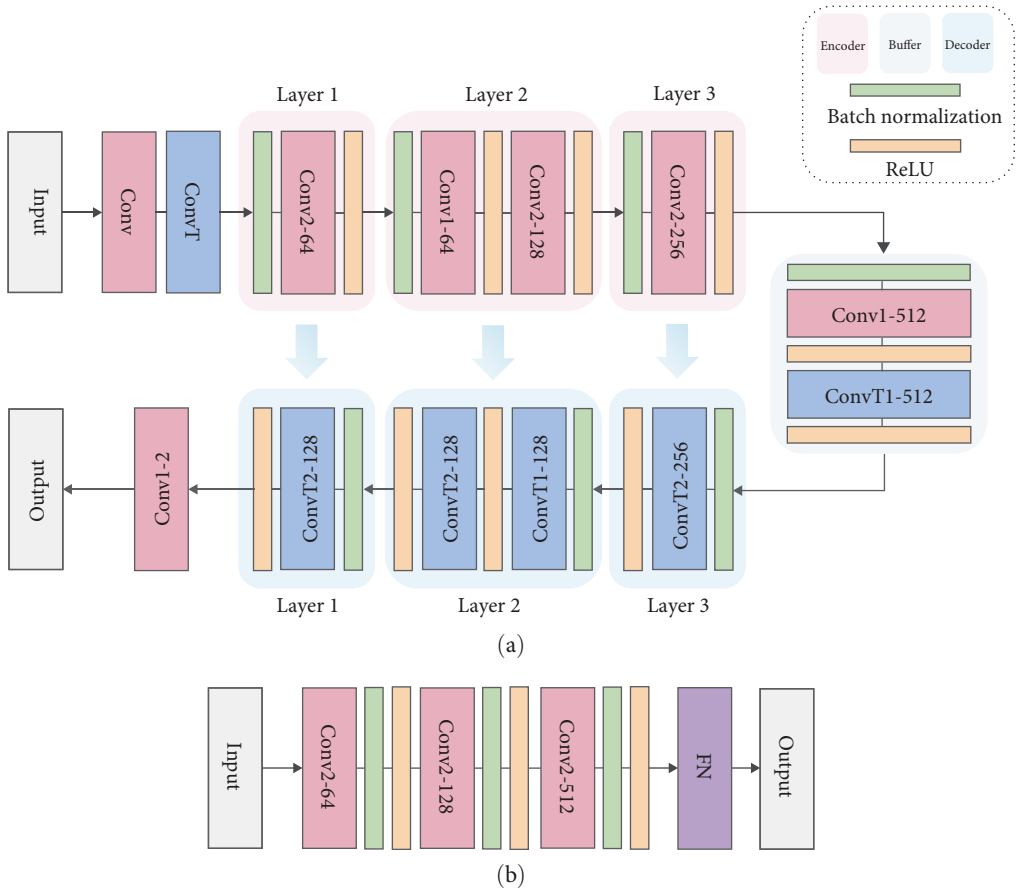

FIGURE 5: PC-GAN network structure: (a) generator and (b) discriminator.

over all responses. The final output of the discriminator is an evaluation of the entire image generated by the generator. The patch architecture enhances the ability to identify local details, which is particularly important for the accuracy of MIMO detection. In addition, we added batch normalization and ReLU activation function after the convolution layer to ensure the robust training of the discriminator.

4. Proposed NR-PC-GAN

Based on the PC-GAN detection method, this section proposes the NR-PC-GAN detection method for massive MIMO detection in low-SNR scenarios. NR-PC-GAN achieves multiplexing of noise removal and signal detection with one network, reducing hardware costs. The MIMO system has noise interference in the communication process, adversely affecting the detection accuracy of the detector. The detection performance decreases with the increase of noise power. Assuming that there is no noise interference in the communication process, we define $\mathbf{Y}_p$ as the noiseless received signal matrix received by the BS, and its expression is as follows:

$$\mathbf{Y}_p = \mathbf{HX}. \tag{6}$$

Equation (4) can be rewritten as follows:

$$\mathbf{Y_H} = \mathbf{Y}_p + \mathbf{n}_1. \tag{7}$$

Before the detection, we remove the Gaussian additive white noise $\mathbf{n}_1$ from the noisy signal matrix $\mathbf{Y_H}$ and obtain the noiseless signal matrix $\mathbf{Y}_p$. We transform $\mathbf{Y_H}$ and $\mathbf{Y}_p$ into image tensor Y_H and Y_p of dimension $N \times P \times 2$, respectively, and use the PC-GAN with image denoising method to obtain the pure received signal. The training of the NR-PC-GAN detection network is divided into two stages: denoise training and detection training.

4.1. Denoise Training. As shown in Figure 6, Y_H is input to the generator, Y_p is input to the discriminator, the generator and the discriminator continuously play minimax game, and the generator is trained to generate $G(Y_H)$, which is similar to Y_p. When the training is completed, the denoiser is obtained.

4.2. Detection Training. We train the detection network with the obtained denoiser, as shown in Figure 7. NR-PC-GAN detection network is basically the same as PC-GAN detection network; the only difference is that the input of generator is no longer Y_H, but the output $\widehat{Y}_p$ of the denoiser.

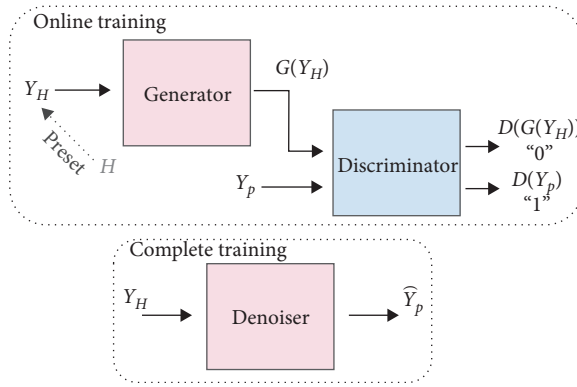

Figure 6: Description of the NR-PC-GAN method for denoise.

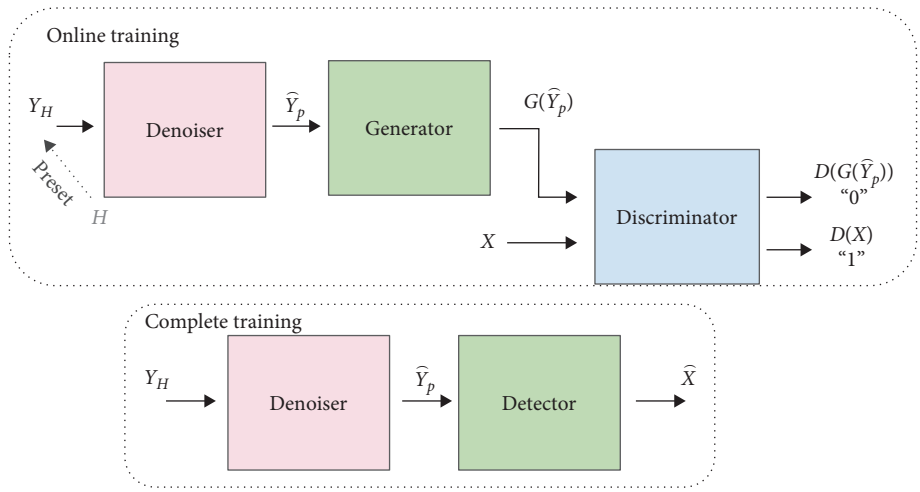

Figure 7: Description of the NR-PC-GAN detection method.

After two training stages, we can use the two trained generators shown in Figure 7 to perform MIMO detection under low SNR. Compared with the PC-GAN detection, NR-PC-GAN detection has been trained twice, and it is straightforward to find that its complexity is twice that of PC-GAN detection. NR-PC-GAN detection achieves improved detection accuracy at the expense of complexity.

5. Simulation and Numerical Results

In this section, we first present the experimental setup and implementation details. Next, numerical results are provided, comparing the detection performance of the proposed detection method with the other detection methods. Then, the contribution of the improved U-Net structure to the detection accuracy and convergence is investigated. Finally, we analyze the complexity of the PC-GAN detection method.

5.1. Implementation Details. In our simulations, the proposed PC-GAN and NR-PC-GAN are implemented in TensorFlow 2.0 with Python [32]. We considered two antenna configurations, 16×64 and, 32×64, and two modulation methods, QPSK and 16QAM. The experimental process is divided into a training phase and a test phase, and the experiment adopts online training mode, i.e., the channel matrices $\mathbf{H}$ in the training and test sets are identical, and 50 samples of $\mathbf{H}$ are generated for each experiment. We consider two channel types, spatially correlated and imperfect CSI.

5.1.1. Spatial Correlation. The spatially correlated channel described by the Kronecker model [33] is as follows:

$$\mathbf{H}_K = \mathbf{R}_N^{1/2} \mathbf{H}_R \mathbf{R}_M^{1/2}, \tag{8}$$

where $\mathbf{H}_R$ is the i.i.d. Rayleigh fading channel, $\mathbf{R}_N^{1/2} \in \mathbb{C}^{N \times N}$ and $\mathbf{R}_M^{1/2} \in \mathbb{C}^{M \times M}$ are the correlation matrices for receiving antenna and single antenna users, respectively, generated according to the exponential correlation model with correlation coefficient $\rho \subset (0,1)$ [17], and the closer ρ is to 1, the stronger the correlation.

5.1.2. Imperfect CSI. Based on the LS (least squares) method for estimating the i.i.d. Rayleigh fading channel to obtain an imperfect channel, we use the normalized mean square error (NMSE) to characterize the difference between the estimated channel matrix and the original channel matrix as follows:

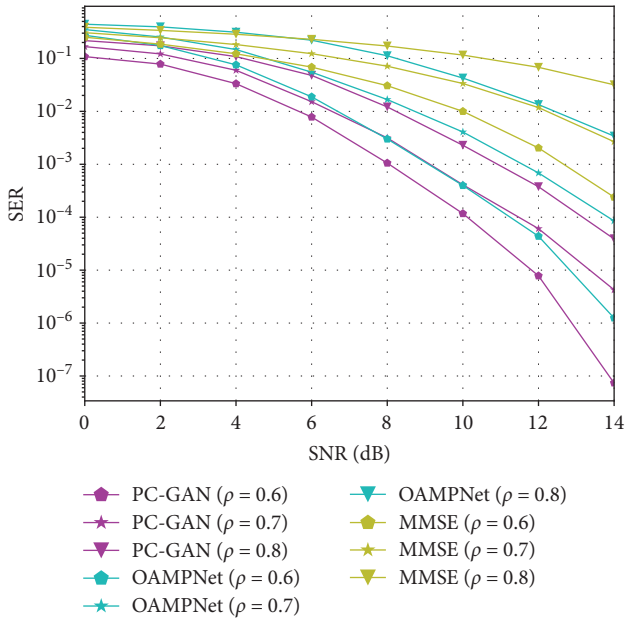

FIGURE 8: SER performance of the proposed PC-GAN with various ρ in a (32, 64) system (i.e., $M = 32$, $N = 64$) using QPSK modulation.

$$\text{NMSE} = 10\log_{10}\left(\text{E}\frac{\left\|\mathbf{H} - \widehat{\mathbf{H}}\right\|^2}{\|\mathbf{H}\|^2}\right), \tag{9}$$

where $\|\bullet\|$ denotes the matrix norm, and we compute $10\log_{10}(\bullet)$ to obtain the NMSE value in dB.

In our work, a total of nine MIMO detectors, PC-GAN, NR-PC-GAN, OAMPNet, MMNet, DetNet, ScNet, LcgNet, DL-based, and MMSE, are simulated. We construct the training set and test set by following a random normal distribution and generating the transmitted signal from the corresponding constellation set (QPSK or 16QAM). The received signal is transmitted over a channel and carries noise. The size of the training set for PC-GAN and NR-PC-GAN is 2,500, and the training process is iterated 20 times with a batch size of 10 for each iteration, while the size of the training set for other networks is 200,000, and the training iterations are 20,000, with a batch size of 500 for each iteration. All networks were evaluated using a test dataset of 20,000 samples. We set the number of network layers to 10 for OAMPNet, MMNet, LcgNet, and DL-based, 30 for DetNet and ScNet, a single-layer structure for PC-GAN, and NR-PC-GAN equivalent to two-layer PC-GAN.

5.2. PC-GAN Detection Performance Analysis. In this subsection, we investigate the massive MIMO detection performance of PC-GAN in the case of spatially correlated channels and imperfect CSI. In addition, we analyze the robustness of PC-GAN to the scenarios with the various mismatches, including SNR and channel gain mismatches.

5.2.1. SER (Symbol Error Ratio) Performance under Spatially Correlated Channel. Figure 8 compares the SER performance of PC-GAN, OAMPNet, and MMSE with QPSK modulation,

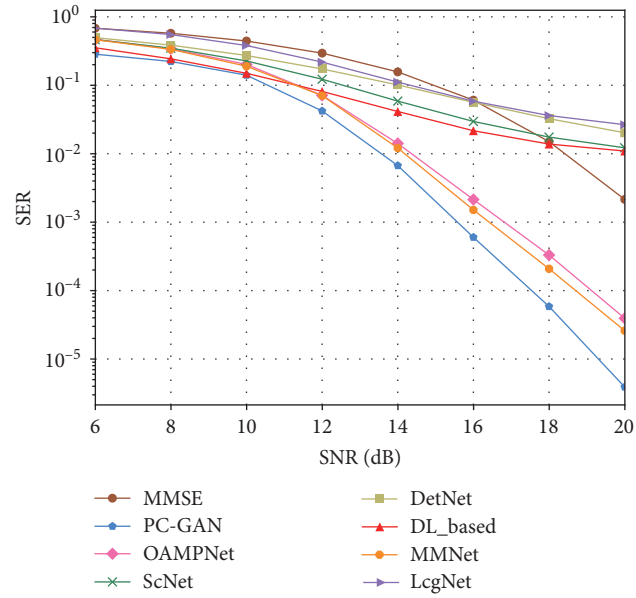

FIGURE 9: SER performance of the proposed PC-GAN at $\rho = 0.5$ in a (32, 64) system (i.e., $M = 32$, $N = 64$) using 16QAM modulation.

correlation coefficients ρ of 0.6, 0.7, and 0.8, and antenna configuration of 32×64. It can be seen that under the same conditions, the PC-GAN detection performance has obvious advantages. Specifically, PC-GAN has 2.4 dB gain over OAMPNet at SER of 10^{-4} under ρ of 0.7. In addition, all the three detectors considered are affected by the channel correlation and show different degrees of degradation in the detection accuracy. OAMPNet detection performance is relatively sensitive to correlation. With the increase in correlation, the detection performance decreases significantly. In contrast, PC-GAN detection is more resistant to correlation. In the case of SER at 10^{-4}, when ρ rises from 0.6 to 0.7, OAMPNet detection performance decreases by 2.6 dB and PC-GAN detection performance decreases by 1.4 dB. When ρ rises from 0.7 to 0.8, PC-GAN detection performance only decreases by 1.8 dB, while OAMPNet is no longer adapted to that condition.

Figure 9 compares the SER performance of the proposed PC-GAN, OAMPNet, MMNet, DetNet, ScNet, LcgNet, DL-based, and MMSE at 16QAM modulation with ρ of 0.5. It can be seen that the proposed PC-GAN can maintain the performance advantage under high-order modulation. The PC-GAN provides performance gains of 1.2 and 1.6 dB compared to MMNet and OAMPNet, respectively, at SNR of 10^{-4}. Next, we analyze the reasons why PC-GAN shows good detection performance under correlated channels. The spatial correlation of the channel causes multiple transmitted signals of MIMO to interfere with each other during transmission, which causes the received signal to change at the BS. When the linear connection between the received and transmitted signal is weakened, the nonlinear connection is enhanced. OAMPNet, MMNet, and other detectors assist traditional linear algorithms with DNN's nonlinear capabilities for detection. The limited nonlinear capability leads to a significant decrease in their detection accuracy with the increase of

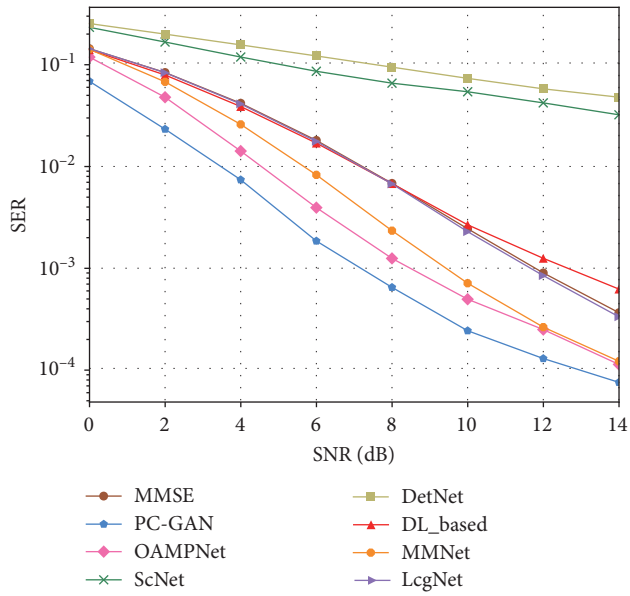

Figure 10: SER performance of the proposed PC-GAN at NMSE = −13 dB in a (32, 64) system (i.e., $M = 32$, $N = 64$) using QPSK modulation.

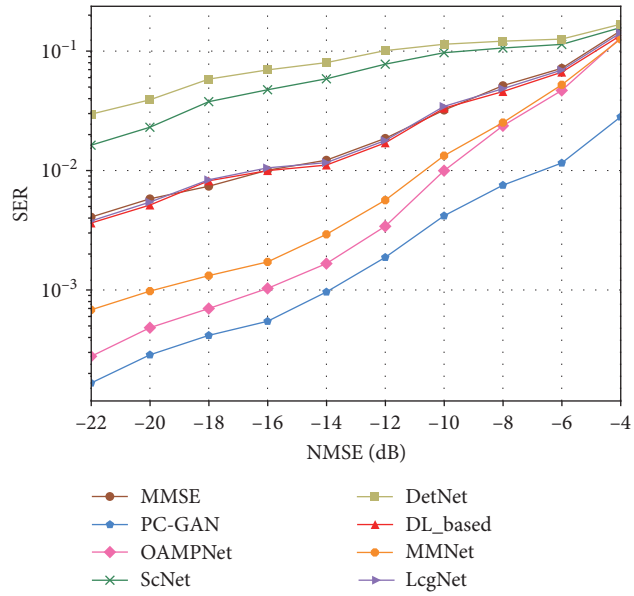

Figure 11: SER performance of the proposed PC-GAN with various NMSE in a (32, 64) system (i.e., $M = 32$, $N = 64$) using QPSK modulation.

channel correlation. The PC-GAN detection method inherits the feature of GAN models that do not require inference during learning [29] and its ability to correct biases introduced by various factors and interactions more easily. Compared with the DNN-based detection algorithm, PC-GAN has stronger nonlinear ability, making it perform well in spatially correlated channels. On the other hand, the small convolution kernel and ReLU function are used in the generator to further enhance the nonlinear capability of the network.

5.2.2. SER Performance under Imperfect CSI. Figure 10 compares the SER performance of PC-GAN, OAMPNet, MMNet, DetNet, ScNet, LcgNet, DL-based, and MMSE, with different SNR for the scenario with QPSK modulation, NMSE of channel estimation being −13 dB, and antenna configuration of 32×64. As shown in Figure 10, PC-GAN outperforms other detectors in the range of SNR from 0to 14 dB. When the detection accuracy SER reaches the level of 10^{-3}, PC-GAN has about 1.4 and 2.3 dB performance gain over OAMPNet and MMNet, respectively. Further, we extend the experiments to show the detection performance of the various detectors under different NMSE. Figure 11 compares the SER performance of various detection methods at different NMES with SNR of 6 dB. PC-GAN achieves superior performance under imperfect CSI, and the gain of PC-GAN over MMNet and OAMPNet is 6 and 2 dB, respectively, when the SER is 10^{-3}. The SER superiority of PC-GAN can be sustained when NMSE changes from −22 to −4 dB. From Figure 11, we can see that the SER advantage of PC-GAN over other detectors gradually increases as the NMSE changes from −22 to −4 dB, which means that the larger the error in the channel estimation, the more PC-GAN can show the performance advantage. Next, we analyze the reasons why PC-GAN exhibits good detection performance under imperfect CSI.

The adaptability of PC-GAN to imperfect CSI stems from the fact that we conditionally preset the CSI. In MIMO detection methods, CSI accuracy directly affects the detection performance. OAMPNet, MMNet, DetNet, ScNet, LcgNet, and DL-based are all DNN-based detection algorithms. For the DNN-based detection algorithms and traditional linear algorithms MMSE, the channel matrix $\mathbf{H}$ is directly involved in the operation as deterministic information during the detection process. In this case, the detection accuracy of these detection methods is positively correlated with the degree of accuracy of $\mathbf{H}$. The lower the degree of accuracy of $\mathbf{H}$, the more significant the decrease in detection accuracy. As can be seen in Figures 10 and 11, the detection accuracy of the DetNet and ScNet detection methods is strongly affected by the imperfect CSI. This is due to the fact that DetNet and ScNet are data-driven detection methods based on which the detection accuracy is more data dependent, and the DetNet and ScNet detection performance is severely degraded when the channel matrix $\mathbf{H}$ is no longer accurate. This further validates that the direct involvement of CSI in the operation is results in the degradation of the detection performance of existing algorithms under imperfect CSI conditions. Our proposed PC-GAN detection method presets the channel matrix $\mathbf{H}$ as a condition in the received signal image Y_H, and realizes MIMO signal detection by constructing a mapping function from the received signal to the transmitted signal. The channel matrix $\mathbf{H}$ is no longer directly involved in the detection process, which effectively resists the impact of imperfect CSI on the detection performance.

5.2.3. Robustness. To verify the robustness of PC-GAN detection, we train PC-GAN under a specific SNR of 12 dB and test its detection performance under the SNR ranging from 0 to 12 dB, to investigate the impact of SNR mismatch on the

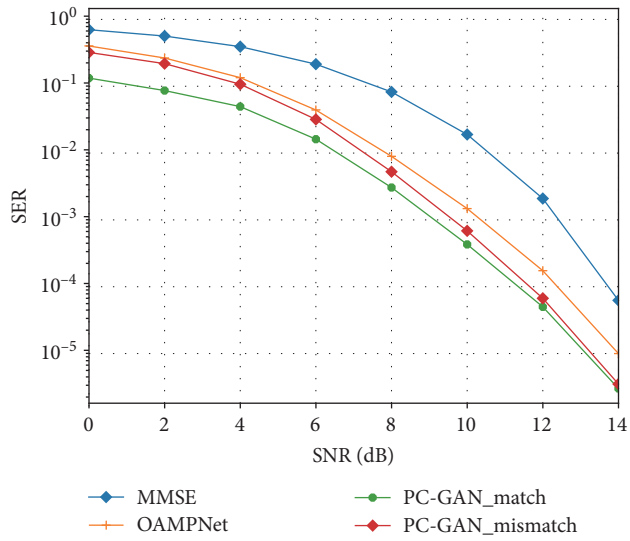

Figure 12: SER performance of the proposed PC-GAN in a (16, 64) system (i.e., $M = 16$, $N = 64$) using 16QAM modulation in the presence of noise mismatch.

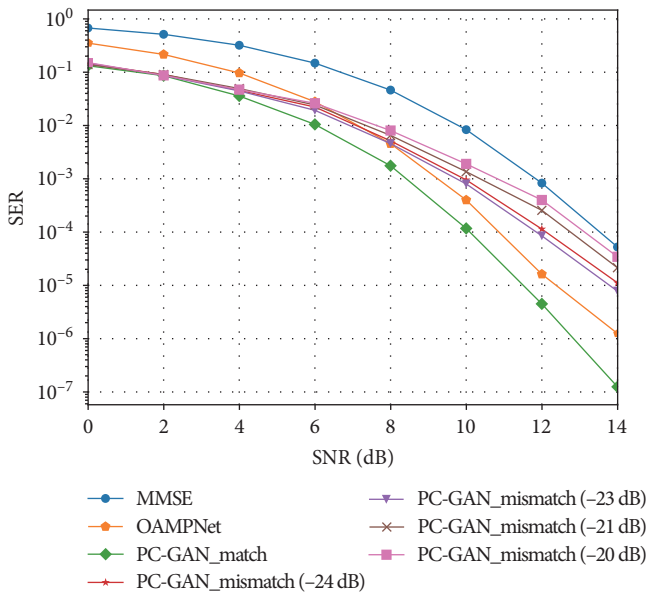

Figure 13: SER performance of the proposed PC-GAN in a (16, 64) system (i.e., $M = 16$, $N = 64$) using 16QAM modulation in the presence of channel mismatch.

detection performance. Similarly, to verify the robustness of PC-GAN detection against imperfect CSI, we train PC-GAN under an imperfect CSI with NMSE of −22 dB and test its detection performance under imperfect CSI with NMSE of −24, −23, −21, and −20 dB. Figures 12 and 13 show the detection results of PC-GAN in SNR and NMSE mismatch states with 16QAM modulation, $\rho = 0.5$, and 16×64 antenna configuration.

As shown in Figure 13, when the SNR is near 12 dB, the detection performance of the mismatched network is almost the same as that of the matched network; when the SNR is far

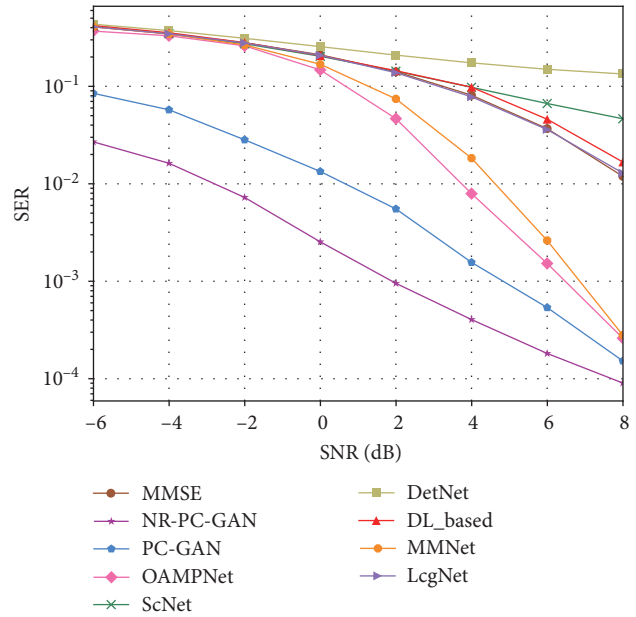

Figure 14: SER performance of the proposed NR-PC-GAN in a (32, 64) system (i.e., $M = 32$, $N = 64$) using QPSK modulation.

below 12 dB, the SER performance curve of the mismatched network gradually deviates from the matched network. Generally speaking, mismatch has little effect on the detection capability of PC-GAN. In Figure 12, when SER is at 10^{-4}, the mismatched network decreases about 0.4 dB compared with the matched network and has about 0.8 dB gain compared with OAMPNet. It can be seen from Figure 13 that when the mismatched NMSE is −21 and −20 dB, the degree of detection performance degradation is large, and when the mismatched NMSE is −24 and −23 dB, the degree of detection performance degradation is small. This means that the channel estimation error is smaller during testing than during training, which can mitigate the impact of channel mismatch on SER performance to a certain extent. When SER is 10^{-4}, the SNR of the network with mismatched NMSE of −23 dB is about 2 dB lower than that of the matched network, but still shows a gain of 1.7 dB compared to the MMSE detector. It can be seen that the impact of channel mismatch on the detection performance is within an acceptable range.

5.3. NR-PC-GAN Detection Performance Analysis. In this section, we study the massive MIMO detection performance of NR-PC-GAN under the condition of high-noise power and show the results of the denoiser. Figure 14 shows the SER performance of NR-PC-GAN, PC-GAN, and other detectors with the setting of QPSK modulation, antenna configuration of 32×64, $\rho = 0.5$, and SNR ranging from −6 to 8 dB. It is clear that NR-PC-GAN performs superiorly at low SNR. When the SNR is 2 dB, the detection SER can reach 10^{-3}, while PC-GAN and OAMPNet achieve the same SER performance with SNR of 4.9 and 7.4 dB, respectively. In addition, compared to PC-GAN, the advantage of NR-PC-GAN gradually decreases with the increase of SNR because the advantage of denoise network is no longer evident with the increase of SNR. In this case, no improvement in

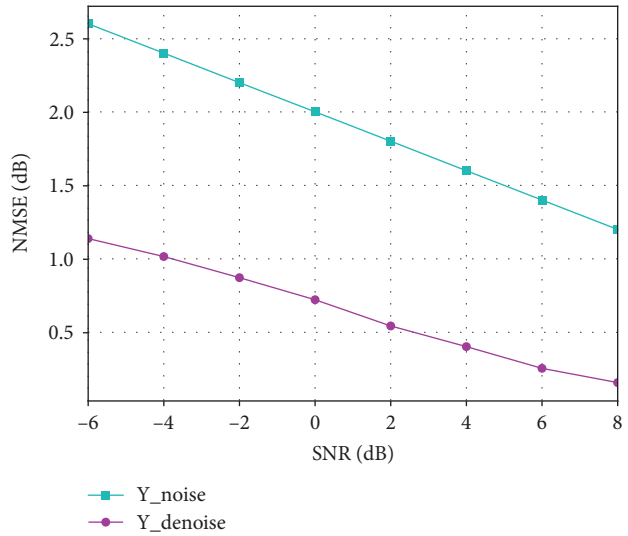

FIGURE 15: Denoising performance of the proposed NR-PC-GAN in a (32, 64) system (i.e., $M = 32$, $N = 64$) using QPSK modulation.

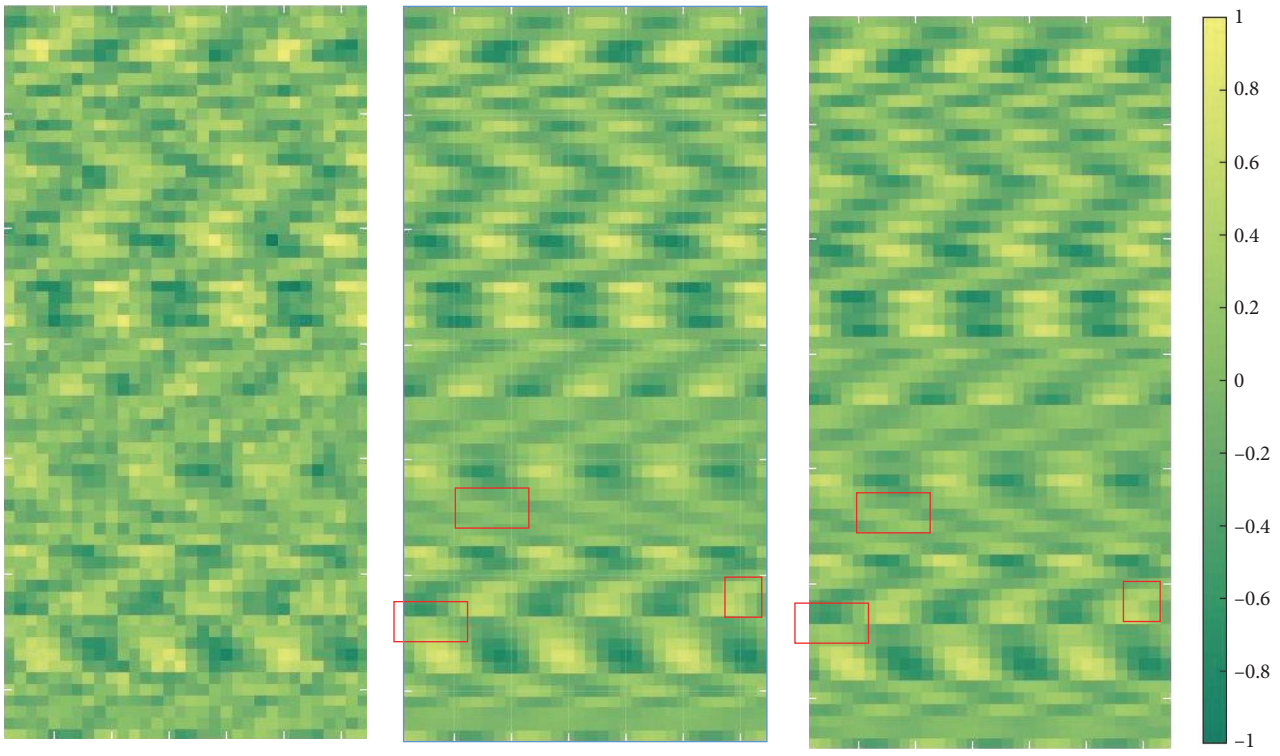

FIGURE 16: (a) noised signal image Y_H, (b) noiseless signal imageY_p, and (c) denoiser generated image $\widehat{Y}_p$.

detection performance can be achieved even with the addition of denoising. Therefore, NR-PC-GAN is more suitable for high-noise channels.

There are two curves in Figure 15; Y_noise indicates the difference between the noisy signal image Y_H and the noiseless signal image Y_p. Y_denoise indicates the difference between the image $\widehat{Y}_p$ generated by the denoiser and the noiseless signal imageY_p, and the NMSE values are obtained as follows.

$$\mathrm{NMSE} = \log_{10}\left(\mathrm{E}\frac{\left\|Y_H or \widehat{Y}_p - Y_p\right\|^2}{\left\|Y_p\right\|^2}\right). \tag{10}$$

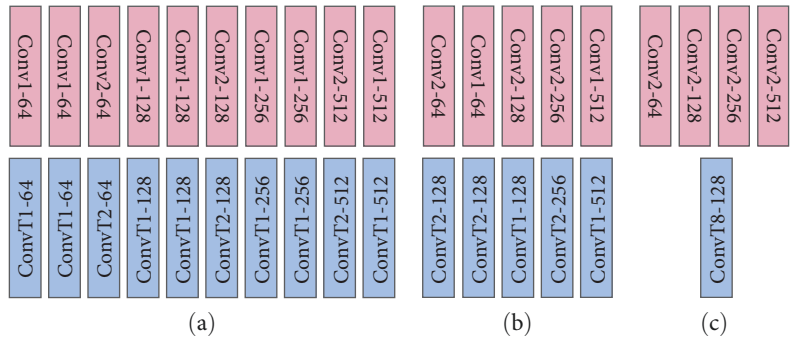

Figure 17: Schematic diagram of generator structure (a) U-Net, (b) improved U-Net, and (c) FCN.

It can be seen that the difference between $\widehat{Y}_p$ and Y_p is much lower than the difference between Y_H and Y_p. Figure 16 shows Y_H, $\widehat{Y}_p$, and Y_p at SNR of −6 dB, and it can be seen that Y_H is quite different from Y_p. The denoiser restores the picture texture by removing the noise and generates $\widehat{Y}_p$, which is very similar to Y_p. There is a tiny difference between Y_p and $\widehat{Y}_p$, which shows that the denoiser can effectively remove the noise. In addition, as shown in Figure 15, with the increase in SNR, the gap between the two curves decreases. The difference between the two curves is 1.4 dB at an SNR of −6 dB, while the difference is about 1.1 dB at an SNR of 8 dB. This further shows that NR-PC-GAN has better performance at low SNR.

5.4. The Contribution of Improved U-Net. We set the experimental conditions to QPSK modulation, ρ equal to 0.6, and the antenna configuration of 32×64. We compare the SER performance of PC-GAN detectors with different iterations when the generator adopts the U-Net structure, the FCN structure and the improved U-Net structure, respectively, and analyze the effect of the improved U-Net on the SER performance and convergence of PC-GAN detection methods. The experimental conditions were kept consistent except for the generator structure. A comparison of the main operations of the encoder and decoder of the original U-Net, FCN, and improved U-Net is given in Figure 17. It can be concluded that the original U-Net decoder and encoder are strictly symmetric; the improved U-Net decoder and encode have the same number of layers, but the numbers of feature maps are no longer perfectly symmetric. In contrast, FCN is a completely asymmetric structure. As shown in Figure 18, the U-Net structure converges after 15 iterations, whereas the improved U-Net and FCN need 19 and 25 iterations, respectively, to reach convergence. This is because the decoder of FCN has only one deconvolution, while the decoder of U-Net is strictly opposite to the encoder, which is a structure of step-by-step amplification, and the superposition of multiple deconvolution operations speeds up the convergence of network. Therefore, the symmetry of the generator decoder and encoder is the main reason for the convergence speed. However, the U-Net structure is trained with fewer samples, and too many convolution operations cause overfitting, significantly damaging the SER performance of detection. Our improved U-Net halves the number

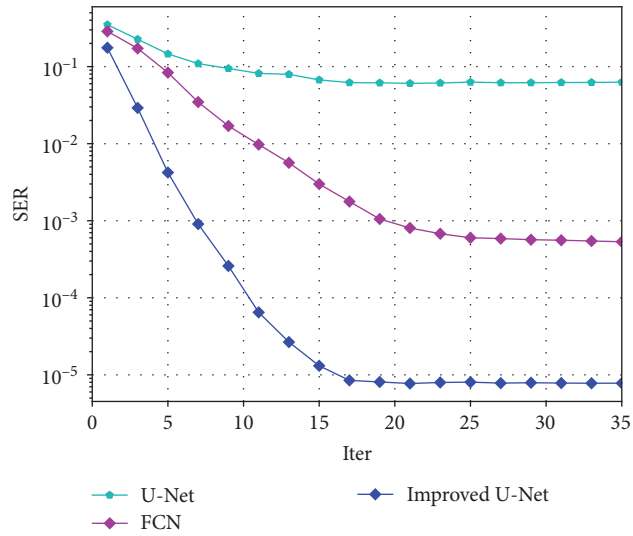

Figure 18: Comparison of convergence of U-Net, FCN, and improved U-Net.

of convolution operations compared to the original U-Net, effectively avoiding overfitting. It can be observed that the SER performance of the improved U-Net reaches below 10^{-5} when the network is converged, while that of the original U-Net and FCN is 10^{-1} and 10^{-3}, respectively. Such a significant performance improvement is also attributed to the enhanced decoder feature reconstruction capability of the improved U-Net.

5.5. Complexity Analysis. In this subsection, the number of operations of the proposed detection network is compared with the other detection networks. As we know, the complexity of detection algorithms mainly comes from multiplication operations. In Table 1, we roughly estimate the number of multiplication operations for DetNet, ScNet, LcgNet, DL-based, MMNet, and the PC-GAN as well as NR-PC-GAN proposed in this paper, using the QPSK modulation method as an example. The OAMPNet algorithm requires matrix inversion operations at each iteration, with a computational complexity of $O(LM^3)$, much higher than the other methods.

In the DNN-based detection algorithm, the computational complexity mainly consists of two parts: initialization

Table 1: The number of multiplications.

Scheme	Multiplication
PC-GAN	$\prod_{i=1}^{13 \text{ or } 16} C_{\text{in}}^{i} C_{\text{out}}^{i} d^2 \text{mw}$
NR-PC-GAN	$2\prod_{i=1}^{13 \text{ or } 16} C_{\text{in}}^{i} C_{\text{out}}^{i} d^2 \text{mw}$
DetNet	$4MN + 8NM^2 + (24M^2 + 4MN + 4M)L$
ScNet	$4MN + 8NM^2 + (12M^2 + 4MN + 4M)L$
LcgNet	$4MN + 8NM^2 + (4M^2 + 6M)L$
DL-based	$4MN + 8NM^2 + (4M^2 + 4MN + 2N + 10M)L$
MMNet	$8MN + (8NM^2 + 4M^2 + 20MN + 2N + 2M)L$

and network iteration process. For example, DetNet needs to calculate $\mathbf{H^T y}$ and $\mathbf{H^T H}$ during initialization, which require $4MN$ and $8NM^2$ operations, respectively, while $(24M^2 + 4MN + 4M)L$ is the number of operations for iteration process, and L is the number of iterative layers. The PC-GAN complexity expression differs from the other networks. As shown in Table 1, d is the number of convolution kernels, m and w are the image length and width, C_{in}^{i} and C_{out}^{i} are the number of the i-th convolution/deconvolution input and output feature maps (the total number of convolution and deconvolution during training and detection is 16 and 13, respectively). In the detection process, PC-GAN convolution brings about 10 times more operations than in DetNet detection. However, in the training process, because PC-GAN uses improved U-Net, only a small number of iterations and a small number of batches per iteration are needed to complete the training. DetNet completes training with 1,000 times more iterations than PC-GAN and 50 times more batches per iteration than PC-GAN. Because we use an online training scheme, the complexity advantage of the PC-GAN method is significant. In addition, NR-PC-GAN is equivalent to performing PC-GAN twice, so the computational complexity is twice that of PC-GAN.

6. Conclusions

In this paper, we propose a PC-GAN for massive MIMO detection. In order to make the CSI no longer directly involved in the detection process, PC-GAN presets the CSI as a condition in the received signal to perform MIMO signal detection in the form of learning the probability distribution of the transmitted signal. To improve the nonlinear capability of the network, we use a small convolutional kernel and a ReLU function in the generator. In addition, to make the detection adaptive to low-SNR scenarios, we propose NR-PC-GAN with a denoising function to gain detection performance by removing the noise in the received signal. Numerical results show that the detection accuracy of PC-GAN under spatially correlated channels and imperfect CSI can surpass that of OAMPNet and MMNet, which are the representative detection methods among the existing works. Moreover, with online training mode, the complexity of PC-GAN can be reduced by several thousand times compared to the DNN-based detection method. In addition, NR-PC-GAN demonstrates superior detection performance in scenarios with high-noise power.

Data Availability

The authors will supply the relevant data in response to reasonable requests.

Conflicts of Interest

The authors declare that there is no conflict of interest regarding the publication of this paper.

Acknowledgments

This work was supported by the Fundamental Research Funds for the Central Universities (grant number: 3072022CF0802).

References

[1] M. S. J. Singha, W. S. W. Saleha, A. T. Abedc, and M. A. Fauzi, "A review on massive MIMO antennas for 5G communication systems on challenges and limitations," *Jurnal Kejuruteraan*, vol. 35, no. 1, pp. 95–103, 2023.

[2] F. Rusek, D. Persson, B. K. Lau, E. G. Larsson, T. L. Marzetta, and F. Tufvesson, "Scaling UP MIMO: opportunities and challenges with very large arrays," *IEEE Signal Processing Magazine*, vol. 30, no. 1, pp. 40–60, 2013.

[3] Z. Guo and P. Nilsson, "Algorithm and implementation of the K-best sphere decoding for MIMO detection," *IEEE Journal on Selected Areas in Communications*, vol. 24, no. 3, pp. 491–503, 2006.

[4] Z.-Q. Luo, W.-K. Ma, A. So, Y. Ye, and S. Zhang, "Semidefinite relaxation of quadratic optimization problems," *IEEE Signal Processing Magazine*, vol. 27, no. 3, pp. 20–34, 2010.

[5] C. Jeon, R. Ghods, A. Maleki, and C. Studer, "Optimality of large MIMO detection via approximate message passing," in *2015 IEEE International Symposium on Information Theory (ISIT)*, pp. 1227–1231, IEEE, Hong Kong, China, June 2015.

[6] J. Ma and L. Ping, "Orthogonal AMP," *IEEE Access*, vol. 5, pp. 2020–2033, 2017.

[7] S. Dorner, S. Cammerer, J. Hoydis, and Sten Brink, "Deep learning based communication over the air," *IEEE Journal of Selected Topics in Signal Processing*, vol. 12, no. 1, pp. 132–143, 2018.

[8] L. V. Nguyen, N. T. Nguyen, N. H. Tran, M. Juntti, A. L. Swindlehurst, and D. H. N. Nguyen, "Leveraging deep neural networks for massive MIMO data detection," *IEEE Wireless Communications*, vol. 30, no. 1, pp. 174–180, 2023.

[9] N. Samuel, T. Diskin, and A. Wiesel, "Deep MIMO detection," 2017.

[10] V. Corlay, J. J. Boutros, P. Ciblat, and L. Brunel, "Multilevel MIMO detection with deep learning," in *2018 52nd Asilomar Conference on Signals, Systems, and Computers*, pp. 1805–1809, IEEE, Pacific Grove, CA, USA, October 2018.

[11] G. Gao, C. Dong, and K. Niu, "Sparsely connected neural network for massive MIMO detection," in *2018 IEEE 4th International Conference on Computer and Communications (ICCC)*, pp. 397–402, IEEE, Chengdu, China, December 2018.

[12] Y. Yu, J. Wang, and L. Guo, "Multisegment mapping network for massive MIMO detection," *International Journal of Antennas and Propagation*, vol. 2021, Article ID 9989634, 7 pages, 2021.

[13] Y. Wei, M.-M. Zhao, M. Hong, M.-J. Zhao, and M. Lei, "Learned conjugate gradient descent network for massive MIMO detection," in *ICC 2020 - 2020 IEEE International*

Conference on Communications (ICC), pp. 1–6, IEEE, Dublin, Ireland, June 2020.

[14] J. Liao, J. Zhao, F. Gao, and G. Y. Li, "A model-driven deep learning method for massive MIMO detection," *IEEE Communications Letters*, vol. 24, no. 8, pp. 1724–1728, 2020.

[15] B. Yin, M. Wu, J. R. Cavallaro, and C. Studer, "Conjugate gradient-based soft-output detection and precoding in massive MIMO systems," in *2014 IEEE Global Communications Conference*, pp. 3696–3701, IEEE, Austin, TX, USA, December 2014.

[16] H. He, C.-K. Wen, S. Jin, and G. Y. Li, "Model-driven deep learning for MIMO detection," *IEEE Transactions on Signal Processing*, vol. 68, pp. 1702–1715, 2020.

[17] M. Khani, M. Alizadeh, J. Hoydis, and P. Fleming, "Adaptive neural signal detection for massive MIMO," *IEEE Transactions on Wireless Communications*, vol. 19, no. 8, pp. 5635–5648, 2020.

[18] J. Liao, J. Zhao, F. Gao, and G. Y. Li, "Deep learning aided low complex sphere decoding for MIMO detection," *IEEE Transactions on Communications*, vol. 70, no. 12, pp. 8046–8059, 2022.

[19] T.-W. Mo, R. Y. Chang, and T.-Y. Kan, "DeepMCTS: deep reinforcement learning assisted Monte Carlo tree search for MIMO Detection," in *2022 IEEE 95th Vehicular Technology Conference: (VTC2022-Spring)*, pp. 1–6, IEEE, Helsinki, Finland, June 2022.

[20] I. J. Goodfellow, J. Pouget-Abadie, M. Mirza et al., "Generative adversarial nets," in *Proceedings of the 27th International Conference on Neural Information Processing Systems*, pp. 2672–2680, MIT Press, Cambridge, MA, USA, 2014.

[21] R. A. Yeh, C. Chen, T. Y. Lim, A. G. Schwing, M. Hasegawa-Johnson, and M. N. Do, "Semantic Image Inpainting with Deep Generative Models," in *2017 IEEE Conference on Computer Vision and Pattern Recognition (CVPR)*, pp. 6882–6890, IEEE, Honolulu, HI, USA, July 2017.

[22] W. Liu, X. Liu, H. Ma, and P. Cheng, "Beyond human-level license plate super-resolution with progressive vehicle search and domain priori GAN," in *Proceedings of the 25th ACM international conference on Multimedia (MM '17)*, pp. 1618–1626, Association for Computing Machinery, New York, NY, USA, 2017.

[23] W. Lijun, Z. Minghong, H. Yu, and S. Lei, "A Signal Demodulation Algorithm Based on Generative Adversarial Networks," in *2021 IEEE 3rd International Conference on Civil Aviation Safety and Information Technology (ICCASIT)*, pp. 1146–1150, IEEE, Changsha, China, October 2021.

[24] H. Ye, L. Liang, G. Y. Li, and B.-H. Juang, "Deep learning-based end-to-end wireless communication systems with conditional GANs as unknown channels," *IEEE Transactions on Wireless Communications*, vol. 19, no. 5, pp. 3133–3143, 2020.

[25] B. Zhang, D. Hu, J. Wu, and Y. Xu, "An effective generative model based channel estimation method with reduced overhead," *IEEE Transactions on Vehicular Technology*, vol. 71, no. 8, pp. 8414–8423, 2022.

[26] Y. Dong, H. Wang, and Y.-D. Yao, "Channel estimation for one-bit multiuser massive MIMO using conditional GAN," *IEEE Communications Letters*, vol. 25, no. 3, pp. 854–858, 2021.

[27] O. Ronneberger, P. Fischer, and T. Brox, "U-Net: convolutional networks for biomedical image segmentation," in *Medical Image Computing and Computer-Assisted Intervention—MICCAI 2015*, N. Navab, J. Hornegger, W. Wells, and A. Frangi, Eds., vol. 9351 of *MICCAI 2015. Lecture Notes in Computer Science*, pp. 234–241, Springer, Cham, 2015.

[28] J. F. Nash Jr., "Equilibrium points in *n*-person games," *Proceedings of the National Academy of Sciences*, vol. 36, no. 1, pp. 48-49, 1950.

[29] M. Mirza and S. Osindero, "Conditional Generative Adversarial Nets," Computer Science, pp. 2672–2680, 2014.

[30] E. Shelhamer, J. Long, and T. Darrell, "Fully convolutional networks for semantic segmentation," *IEEE Transactions on Pattern Analysis and Machine Intelligence*, vol. 39, no. 4, pp. 640–651, 2017.

[31] P. Isola, J.-Y. Zhu, T. Zhou, and A. A. Efros, "Image-to-image translation with conditional adversarial networks," in *2017 IEEE Conference on Computer Vision and Pattern Recognition (CVPR)*, pp. 5967–5976, IEEE, Honolulu, HI, USA, 2017.

[32] M. Abadi, P. Barham, J. Chen et al., "TensorFlow: a system for large-scale machine learning," in *Proceedings of the 12th USENIX Conference on Operating Systems Design and Implementation (OSDI'16)*, pp. 265–283, USENIX Association, USA, 2016.

[33] K. Yu, M. Bengtsson, B. Ottersten, D. McNamara, P. Karlsson, and M. Beach, "Modeling of wide-band MIMO radio channels based on NLoS Indoor measurements," *IEEE Transactions on Vehicular Technology*, vol. 53, no. 3, pp. 655–665, 2004.